




## RESEARCH ARTICLE

# Dual-frequency irradiation CEST-MRI of endogenous bulk mobile proteins

Steffen Goerke<sup>1</sup>  | Johannes Breitling<sup>1</sup> | Moritz Zaiss<sup>1,2</sup>  | Johannes Windschuh<sup>1</sup> | Patrick Kunz<sup>3</sup> | Patrick Schuenke<sup>1</sup> | Daniel Paech<sup>4</sup> | Dario L. Longo<sup>5</sup>  | Karel D. Klika<sup>6</sup> | Mark E. Ladd<sup>1,7,8</sup> | Peter Bachert<sup>1,7</sup>

<sup>1</sup>Division of Medical Physics in Radiology, German Cancer Research Center (DKFZ), Heidelberg, Germany

<sup>2</sup>Department of High-field Magnetic Resonance, Max-Planck-Institute for Biological Cybernetics, Tübingen, Germany

<sup>3</sup>Division of Functional Genome Analysis, German Cancer Research Center (DKFZ), Heidelberg, Germany

<sup>4</sup>Department of Radiology, German Cancer Research Center (DKFZ), Heidelberg, Germany

<sup>5</sup>Institute of Biostructure and Bioimaging (IBB), National Research Council (CNR), Torino, Italy

<sup>6</sup>Molecular Structure Analysis, German Cancer Research Center (DKFZ), Heidelberg, Germany

<sup>7</sup>Department of Physics and Astronomy, University of Heidelberg, Heidelberg, Germany

<sup>8</sup>Faculty of Medicine, University of Heidelberg, Heidelberg, Germany

**Correspondence**

S. Goerke, Division of Medical Physics in Radiology, German Cancer Research Center (DKFZ), Im Neuenheimer Feld 280, 69120 Heidelberg, Baden-Württemberg, Germany. Email: s.goerke@dkfz.de

A novel MRI contrast is proposed which enables the selective detection of endogenous bulk mobile proteins *in vivo*. Such a non-invasive imaging technique may be of particular interest for many diseases associated with pathological alterations of protein expression, such as cancer and neurodegenerative disorders. Specificity to mobile proteins was achieved by the selective measurement of intramolecular spin diffusion and the removal of semi-solid macromolecular signal components by a correction procedure. For this purpose, the approach of chemical exchange saturation transfer (CEST) was extended to a radiofrequency (RF) irradiation scheme at two different frequency offsets (dualCEST). Using protein model solutions, it was demonstrated that the dualCEST technique allows the calculation of an image contrast which is exclusively sensitive to changes in concentration, molecular size and the folding state of mobile proteins. With respect to application in humans, dualCEST overcomes the selectivity limitations at relatively low magnetic field strengths, and thus enables examinations on clinical MR scanners. The feasibility of dualCEST examinations in humans was verified by a proof-of-principle examination of a brain tumor patient at 3 T. With its specificity for the mobile fraction of the proteome, its comparable sensitivity to conventional water proton MRI and its applicability to clinical MR scanners, this technique represents a further step towards the non-invasive imaging of proteomic changes in humans.

**KEYWORDS**

cancer, CEST, magnetization transfer, MRI, proteins, spin diffusion

**Abbreviations used:** AREX, apparent exchange-dependent relaxation;  $B_0$ , magnetic field strength;  $B_1$ , RF amplitude; BSA, bovine serum albumin; CEST, chemical exchange saturation transfer; CSF, cerebrospinal fluid; DC, duty cycle; dualCEST, dual-frequency irradiation CEST;  $M_0$ , equilibrium water magnetization;  $M_{\text{sat}}$ , water magnetization after pre-saturation; MW, molecular weight; off, far off-resonant frequency offset; PBS, phosphate-buffered saline;  $R_{1\text{obs}}$ , observed longitudinal relaxation rate of water; RF, radiofrequency; rNOE, relayed nuclear Overhauser effect; SAR, specific absorption rate; SDS, sodium dodecyl sulfate; SNR, signal-to-noise ratio; ssMT, semi-solid magnetization transfer;  $T_{1\text{obs}}$ , observed longitudinal relaxation time of water;  $T_{\Delta\omega\text{C}}(\Delta\omega)$ , saturation crosstalk;  $t_p$ , pulse length;  $t_d$ , interpulse delay;  $t_{\text{sat}}$ , saturation length;  $T_{\text{protein}}$ , isolated saturation crosstalk of mobile proteins;  $T_{\text{ssMT}}$ , isolated saturation crosstalk of semi-solid macromolecular structures; Z, Z-spectrum;  $Z_{\text{ref}}$ , reference Z-spectrum;  $\Delta\omega$ , frequency offset;  $\Delta\omega_{\text{C}}$ , constant frequency offset.

Steffen Goerke and Johannes Breitling contributed equally to this work.

## 1 | INTRODUCTION

Chemical exchange saturation transfer (CEST) MRI has emerged as an important contrast mechanism for the detection of low concentration solutes, such as proteins or small metabolites in living tissue.<sup>1-5</sup> CEST exploits the spontaneous chemical exchange of protons in order to indirectly detect the solutes via the abundant water proton signal. This is realized by a frequency-selective pre-saturation of chemically exchanging protons in solutes and a subsequent fast MRI readout of the water signal. The indirect detection generates a signal amplification enabling, in principle, high-resolution imaging of solutes with a sensitivity comparable to normal water proton MRI.

However, in living tissue diverse CEST signals of different cellular compounds, such as proteins,<sup>6-9</sup> small metabolites,<sup>10-15</sup> lipids<sup>16,17</sup> and semi-solid macromolecular structures,<sup>18-20</sup> spectrally overlap in the Z-spectrum (Figure 1B). Moreover, CEST signals depend on the rate of chemical exchange, which in turn is determined by various physiological parameters, in particular pH and temperature.<sup>3,21-23</sup> On the one hand, this multi-parametric dependence makes CEST a valuable imaging technique with the potential to depict a wide range of physiological processes, but, on the other, the numerous parameters are also a strong drawback in terms of specificity. Although specific adjustments of the CEST pulse scheme (e.g. tuning of the pre-saturation amplitude  $B_1$  or the interpulse delay  $t_d$ ) allow the design of exchange rate filters<sup>24-26</sup> that highlight the signal component of one specific compound, to date a selective detection without contributions from other cellular compounds has not been possible. The introduction of specificity has become one of the most important issues in the research field of CEST-MRI.

Here, we present a novel CEST-based technique – dual-frequency irradiation CEST (dualCEST) – that allows the selective detection of endogenous bulk mobile proteins *in vivo*. Specificity of the dualCEST signal is achieved by the introduction of a novel dimension of selectivity: the detection of the coupling between different CEST signals (Figure 1B). As only mobile proteins possess individual resonances of significant amplitude on both sides of the Z-spectrum that are coupled via a magnetization transfer pathway, exceptional specificity can be achieved by taking advantage of this trait. Signal contributions from the comparatively broad resonance of the semi-solid magnetization transfer (ssMT) can be removed by a correction procedure. Pre-saturation at two different frequency offsets,  $\Delta\omega$  and  $\Delta\omega_C$ , was realized by an alternating radiofrequency (RF) irradiation scheme (Figure 1A).

The terminology 'bulk mobile proteins' is a combination of the specificity of the dualCEST technique to the collective signal of all proteins and the separation of MR signals by their mobility (for a detailed explanation, see the Discussion section). The bulk mobile protein signal comprises mainly cytosolic proteins, many endoplasmic reticulum proteins and secreted proteins.<sup>8</sup> Although the detection of specific protein species is not feasible by this means, the bulk mobile protein signal is expected to be a valuable marker for diseases that are associated with profound alterations of the proteome. Bulk mobile proteins are generally assumed to be the main source of the prominent amide proton resonance at

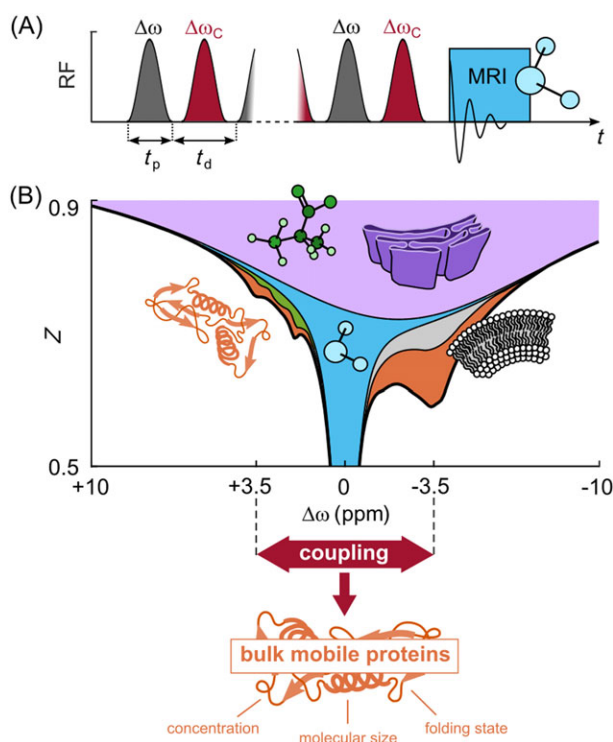


**FIGURE 1** The dual-frequency irradiation chemical exchange saturation transfer (dualCEST) approach. (A) Scheme of the pulse sequence. (B) Z-spectrum of *ex vivo* porcine brain tissue homogenate ( $B_1 = 0.75 \mu\text{T}$ ,  $B_0 = 14.1 \text{ T}$ ). The subdivision of the Z-spectrum into contributions of different cellular compounds is an estimation. dualCEST detects the coupling of different CEST signals, allowing the selection of signals of bulk mobile proteins (orange) from the background of other cellular compounds: metabolites (green), lipids (gray), semi-solid macromolecular structures (purple) and water (blue)

$\Delta\omega = +3.5$  ppm or the relayed nuclear Overhauser effect (rNOE)-CEST signal of aliphatic protons at around  $\Delta\omega = -3.5$  ppm.<sup>6-8,16,17,27-32</sup> These two signals have already been shown to allow the diagnosis of several diverse diseases and to provide decisive information for ongoing therapy. Especially with respect to cancer, CEST imaging at  $\Delta\omega = \pm 3.5$  ppm has enabled the assessment of tumor malignancy,<sup>33</sup> the differentiation between radiation necrosis and tumor progression<sup>34,35</sup> and the detection of disrupted blood-brain barriers without the application of contrast media.<sup>9</sup> Although the value of the amide and aliphatic proton signal has been demonstrated in diverse studies, nevertheless, the underlying origin of the contrast is not completely understood. The technique of dualCEST represents a unique opportunity to determine the actual contribution of mobile proteins to CEST signal changes in pathological tissue, which may lead to new insights into diseases on a molecular level.

This study comprises the introduction of the dualCEST contrast mechanism, a comprehensive optimization of technical parameters, an analytical model of the observed signal, an experimental verification of its specificity to mobile proteins *in vitro* and a proof-of-principle demonstration of its applicability *in vivo*. A detailed analysis of the diagnostic value of the method will be addressed in a future study. With respect to examinations in humans, the exceptional specificity of the presented technique evades the ultra-high static magnetic field strengths  $B_0 \geq 7$  T that are required for the adequate separation of individual resonances in conventional CEST-MRI, thus allowing its straightforward application on clinical MR scanners ( $B_0 \leq 3$  T). Hence, dualCEST enables the selective detection of endogenous bulk mobile proteins at clinical magnetic field strength, providing the potential to be a valuable diagnostic tool to detect aberrant proteomes *in vivo*.

## 2 | MATERIALS AND METHODS

### 2.1 | Model solutions

In total, 42 model solutions containing varying amounts of globular proteins, sodium dodecyl sulfate (SDS), creatine, carnosine, lipids and tissue homogenates were prepared. A detailed list of all experimental parameters is presented in Supporting Information Table S1. Unless otherwise specified, model solutions were buffered at pH 7 using phosphate-buffered saline (PBS). Final pH values were checked by means of a calibrated pH electrode, and deviations from pH 7 (e.g. in the case of high solute concentrations) were corrected using NaOH or HCl. All model solutions were pipetted from highly concentrated stock solutions to ensure the precise adjustment of different concentrations. Samples containing *ex vivo* tissue components were continuously chilled on ice before measurement. Protein-free brain lipids were extracted from mouse brain tissue with tetrahydrofuran, filtered and lyophilized for liposome preparation (size, 120 nm) throughout sonication. Tissue homogenates were obtained from white matter porcine brain tissue and prepared as described in previous studies.<sup>9</sup>

### 2.2 | Subjects

One 57-year-old male patient with newly diagnosed and histopathologically proven glioblastoma (grade IV) was examined before therapy. This study was approved by the local ethics committee of the Medical Faculty of the University of Heidelberg and is in accordance with the relevant guidelines and regulations. Written informed consent was received from the patient prior to the examination.

### 2.3 | CEST spectroscopy

Model solutions were examined on 14.1-T (600 MHz for <sup>1</sup>H) Avance II and 9.4-T (400 MHz for <sup>1</sup>H) Avance III narrow-bore spectrometers (Bruker BioSpin, Karlsruhe-Rheinstetten, Germany). A 5-mm or 8-mm probe was used for RF irradiation and signal acquisition. To avoid radiation damping, the probes were operated detuned. The temperature of the samples was stabilized at 25 or 37°C using the internal heating and cooling device. For conventional CEST measurements, pre-saturation at  $\Delta\omega$  was achieved by Gaussian-shaped RF pulses of mean amplitude  $B_1 = \text{flip angle}/(\gamma \cdot t_p)$ , length  $t_p$  and duty cycle  $DC = t_p/(t_p + t_d)$ . In the case of dualCEST, an additional Gaussian-shaped RF pulse ( $\Delta\omega_c$ ) of the same amplitude and length was centered in the middle of the interpulse delay  $t_d$  (Figure 1A). A detailed list of all experimental parameters is presented in Table S1. The overall duration of the pre-saturation period  $t_{\text{sat}}$  complied with the criterion for steady-state measurements,  $t_{\text{sat}} > 3-4 \cdot T_{1\text{obs}}$ , with the observed longitudinal relaxation time of water  $T_{1\text{obs}}$ .<sup>20</sup> Z-values were calculated by integration of the water resonance in the range of  $\pm 0.45$  ppm ( $M_{\text{sat}}$ ) and normalized with the equilibrium magnetization ( $M_0$ ):  $Z = M_{\text{sat}}/M_0$ . To compensate for systematic signal fluctuations (i.e. caused by the signal amplifier or receiver),  $M_0$  was acquired at different time points and interpolated to obtain an individual  $M_0$  for each pre-saturation cycle. Conventional Z-spectra were sampled at 118 frequency offsets in unequal steps between  $\pm 150$  ppm. Isolated CEST signals, compensated for direct water saturation effects (spillover dilution), ssMT and water relaxation properties, were calculated at each frequency offset  $\Delta\omega$  using the apparent exchange-dependent relaxation (AREX) evaluation<sup>36</sup>:  $\text{AREX}(\Delta\omega) = \frac{R_{1\text{obs}}}{DC} \cdot \left( \frac{1}{Z(\Delta\omega)} - \frac{1}{Z_{\text{ref}}(\Delta\omega)} \right)$ . The observed longitudinal relaxation rate of water

$R_{1\text{obs}} = \frac{1}{T_{1\text{obs}}}$  was measured using a saturation-recovery sequence. The reference spectrum  $Z_{\text{ref}}$  was estimated by a multi-parametric fit:  $Z_{\text{ref}} = 1 - \sum_i L_i$ , where  $L_i$  are Lorentzian-shaped functions representing the direct water saturation and ssMT. To avoid contributions from CEST signals, as well as to take into account the broadening of the direct water saturation as a result of a pulsed pre-saturation, data points in the range from  $\pm 10$  to  $\pm 0.5$  ppm and in between  $\pm 0.2$  ppm were excluded from the fitting procedure. Conventional asymmetry analysis (based on non-fitted

data) was performed by:  $MTR_{\text{asym}}(\Delta\omega) = Z(-\Delta\omega) - Z(\Delta\omega)$ . Depending on the CEST signal strength of the respective evaluation method, measurements were repeated several times (Table S1).

## 2.4 | DualCEST MRI

*In vivo* measurements were performed on a 3-T (123.26 MHz for  $^1\text{H}$ ) whole-body MR-PET tomograph (Biograph mMR; Siemens Healthcare GmbH, Erlangen, Germany) using a custom-developed CEST pulse sequence based on a two-dimensional Half Fourier Acquisition Single Shot Turbo Spin Echo (HASTE) readout and a 16-channel Siemens mMR Head/Neck A Tim Coil.  $M_{\text{sat}}$  images (matrix,  $128 \times 102$ ; resolution,  $1.88 \times 1.88 \times 5 \text{ mm}^3$ ) were acquired after pre-saturation with 84 pairs of Gaussian-shaped RF pulses at  $\Delta\omega$  and  $\Delta\omega_{\text{C}}$  of  $B_1 = 2 \mu\text{T}$ ,  $t_{\text{p}} = 20 \text{ ms}$  and  $\text{DC} = 28\%$ , leading to  $t_{\text{sat}} = 6 \text{ s}$ . All images were corrected for motion artifacts by an intensity-based image registration. Analogous to CEST spectroscopy, several  $M_0$  images were acquired at different time points and interpolated to yield an individual  $M_0$  for each Z-image. To increase the signal-to-noise ratio (SNR), Z-images were averaged over 18 acquisitions and smoothed by a Gaussian kernel ( $\sigma = 1 \text{ pixel}$ ). The final dualCEST contrast (Equation 2) was corrected for  $B_1$  inhomogeneities by means of the one-point 'contrast-correction' method as described in a previous study.<sup>37</sup>  $B_0$  and  $B_1$  were determined by the simultaneous mapping of the water shift and  $B_1$  (WASABI)<sup>38</sup> approach using the same CEST pulse sequence with adjusted pre-saturation parameters.  $T_{1\text{obs}}$  mapping was achieved by fitting  $T_{1\text{obs}}$ -weighted images of a saturation recovery HASTE sequence. In total, the overall measurement time was approximately 22 min, comprising 18 min of dualCEST, 2 min of WASABI and 2 min of  $T_{1\text{obs}}$  mapping.

To investigate the influence of  $B_0$ , the same dualCEST pulse sequence was implemented on a 7-T whole-body MR tomograph (MAGNETOM 7 T; Siemens Healthcare GmbH), but based on a two-dimensional gradient echo (GRE) readout.

## 3 | RESULTS

### 3.1 | The dualCEST approach

To demonstrate the concept of the dualCEST approach, a mobile protein solution containing bovine serum albumin (BSA) was investigated. DualCEST detects the MR signal of water after alternating RF irradiation at two different frequency offsets,  $\Delta\omega$  and  $\Delta\omega_{\text{C}}$  (Figure 1A). This allows the simultaneous sampling of the conventional Z-spectrum as a function of  $\Delta\omega$  while constantly saturating CEST signals at  $\Delta\omega_{\text{C}}$  (Figure 2A). For a

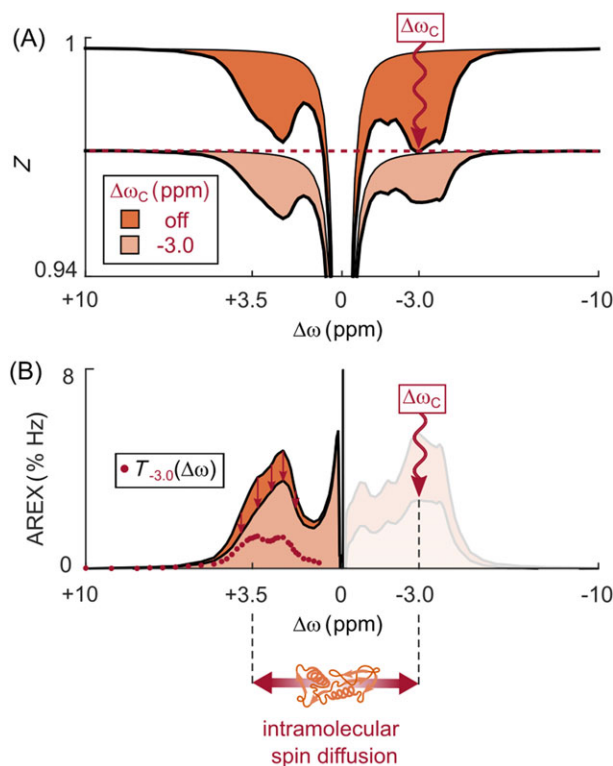


**FIGURE 2** Isolation of the saturation crosstalk. (A) Z-spectra of a mobile protein solution containing BSA ( $B_1 = 0.45 \mu\text{T}$ ,  $B_0 = 14.1 \text{ T}$ ) with and without constant saturation at  $\Delta\omega_{\text{C}}$ . (B) Isolated CEST signals calculated by the AREX evaluation. The saturation crosstalk  $T_{\Delta\omega_{\text{C}}}(\Delta\omega)$  (red dots) is defined by the difference between the two AREX spectra

detailed analysis of the influence of the constant saturation, the CEST signals of proteins were separated from the direct water saturation ( $\Delta\omega = 0$  ppm) by the AREX evaluation<sup>36</sup> (Figure 2B). Constant saturation at  $\Delta\omega_C = -3.0$  ppm led to a significant reduction in protein CEST signals on the opposite side of the water resonance ( $\Delta\omega > 0$  ppm). Hence, protein CEST signals in the positive and negative frequency region are coupled via a magnetization transfer pathway. The amount of magnetization transfer between two particular frequency offsets – in the following, termed as saturation crosstalk  $T_{\Delta\omega_C}(\Delta\omega)$  – can be quantified by subtraction of the AREX spectra. Quantification by simple subtraction of the two spectra is justified because of the linearity of CEST signals using the AREX evaluation. Remarkably, for mobile proteins, the saturation crosstalk is on the order of 30–40% of the conventional AREX spectrum, demonstrating the potential for its application *in vivo*. The observed saturation crosstalk is attributed to intramolecular spin diffusion<sup>39</sup> between dipolar-coupled protons. Spin diffusion is also known to mediate the intramolecular magnetization transfer of rNOE-CEST signals, which have been studied extensively in the past few years.<sup>16,17,26,40</sup>

Rearrangement of the mathematical expression for  $T$  allows the calculation of the saturation crosstalk without the need for prior AREX evaluation (Supporting Information Figure S1):

$$T_{\Delta\omega_C}(\Delta\omega) = \frac{R_{1\text{obs}}}{DC} \cdot \left[ \frac{1}{Z_{\text{off}}(\Delta\omega)} + \frac{1}{Z_{\Delta\omega_C}(\text{off})} - \frac{1}{Z_{\Delta\omega_C}(\Delta\omega)} - \frac{1}{Z_{\text{off}}(\text{off})} \right] \quad (1)$$

where  $Z_{\Delta\omega_C}(\Delta\omega)$  is the Z-value after saturation at  $\Delta\omega$  and  $\Delta\omega_C$ , and the far off-resonant frequency offset,  $\text{off} = 150$  ppm, which is synonymous with disabling of the saturation. This calculation has the advantage that  $T_{\Delta\omega_C}(\Delta\omega)$  can be determined without the need for the estimation of the direct water saturation by a fitting procedure. Consequently, the saturation crosstalk between two particular frequency offsets is characterized by only four Z-values (Equation 1), allowing a fast and direct acquisition which is crucial for application *in vivo*.

In order to maximize the dualCEST signal, its dependence on several technical parameters was investigated.  $T$  monotonically increases as a function of the saturation duration and reaches steady state at  $t_{\text{sat}} \approx 3 \cdot T_{1\text{obs}}$  (Figure 3B). Furthermore,  $T$  is effectively independent of the DC (Figure 3D), in compliance with the AREX evaluation. An unexpected observation is the increase in  $T$  for shorter pulse lengths  $t_p$  (Figure 3F), which thereby provides a simple means to amplify the dualCEST signal. A detailed explanation of this effect is provided in the Discussion section. Remarkably, an increase in  $T$  can also be observed for decreasing magnetic field strengths (Figure 3J), thus enabling the application of the dualCEST technique on clinical MR scanners. In addition,  $B_1$  can be increased to amplify the dualCEST signal (Figure 3H). The monotonic increase is again in coherence with the AREX evaluation. For further investigations on the 14.1-T MR spectrometer,  $t_p = 7.8$  ms and  $B_1 = 1.5$   $\mu\text{T}$  were used, which are optimal in terms of maximizing the signal strength while avoiding an excessive broadening of signals.

The advantage of the dualCEST approach in comparison to conventional CEST is that it provides a novel dimension of selectivity. As dualCEST detects the coupling between two different CEST signals, selectivity to compounds that exhibit more than one resonance in the Z-spectrum can be achieved. Consequently, by setting the two frequency offsets to the positive and negative regions ( $\Delta\omega > 0$  and  $\Delta\omega_C < 0$  ppm), the dualCEST signal is selective to mobile proteins because only mobile proteins offer individual resonances of significant amplitude on both sides of the Z-spectrum (Figure 1B). However, as the comparatively broad resonance of ssMT also ranges from positive to negative frequency offsets, a contribution to the dualCEST signal from macromolecular structures can be expected. To retrieve the isolated signal of mobile proteins, a correction method has to be applied.

### 3.2 | Correction for signals of semi-solid macromolecular structures

To investigate the dualCEST signal of mobile proteins in the presence of semi-solid macromolecular structures, an *ex vivo* tissue homogenate derived from porcine brain was prepared. The corresponding dualCEST spectrum obtained with similar sequence parameters as in Figure 2 ( $\Delta\omega_C = -3.5$  ppm) exhibits a comparatively broad saturation crosstalk with a spectral width larger than 10 ppm (Figure 4B, red line). Hence, the acquired signal comprises, in addition to signals of mobile proteins, a component originating from semi-solid macromolecular structures. To extract the superimposed signal of mobile proteins  $T_{\text{protein}}$ , the selectivity of the dualCEST approach was utilized (Figure 4A): By shifting the constant saturation frequency off-resonance from mobile protein signals while remaining on-resonance for the ssMT ( $\Delta\omega_C = -10$  ppm), the spectral profile of the underlying ssMT component can be sampled in an isolated manner (Figure 4B, magenta line). The actual amplitude of the isolated saturation crosstalk of semi-solid macromolecular structures  $T_{\text{ssMT}}$  (Figure 4B, black line) is determined by scaling the spectral profile by the factor  $T_{-3.5(+10)}/T_{-10(+10)}$  (Figure 4B, gray circles). This calculation is not an estimation but can be derived analytically (Supporting Information Figure S2). It is important to note that the correction method is also independent of the ssMT line shape, allowing application even in the case of an asymmetric ssMT. Overall, the isolated signal of mobile proteins in the presence of semi-solid macromolecular structures can be determined by:

$$T_{\text{protein}}(\Delta\omega) = T_{-3.5}(\Delta\omega) - \underbrace{\frac{T_{-3.5(+10)}}{T_{-10(+10)}}}_{T_{\text{ssMT}}} \cdot T_{-10}(\Delta\omega) \quad (2)$$

Equation 2 enables the application of the dualCEST approach to investigate alterations of bulk mobile proteins in living organisms. For the calculation of  $T_{\text{protein}}$ , altogether nine Z-values are required, which leads to about a doubling in the acquisition time compared with the uncorrected signal (Equation 1). However, a fitting procedure is still not required, allowing the fast determination of  $T_{\text{protein}}$  *in vivo* without the need

to sample an entire spectrum at various  $\Delta\omega$ . The absence of signals  $T_{\text{protein}}$  at frequency offsets larger than 10 ppm (Figure 4B, orange line) indicates proper functioning of the proposed correction procedure. It is worth noting the presence of an asymmetric ssMT in this experiment (Figure 4A, purple region) which does not distract from proper functioning of the correction method. However, to unambiguously verify the assignment of the dualCEST signal to mobile proteins, different cellular compounds were added successively to a protein model solution.

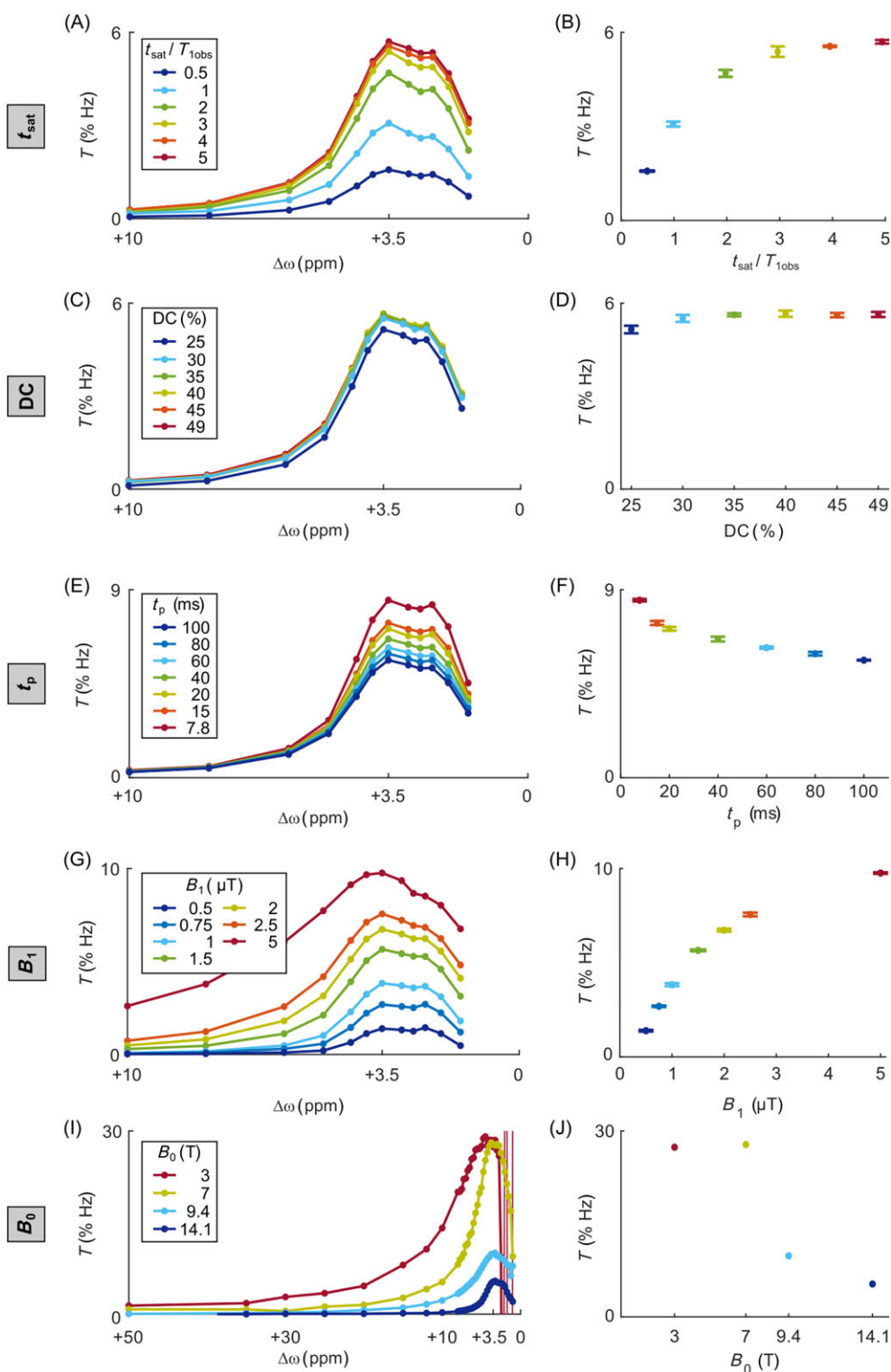


**FIGURE 3** Dependence of the dualCEST signal on technical parameters.  $T$ -spectra of BSA ( $\Delta\omega_C = -3.5$  ppm,  $B_1 = 1.5$   $\mu\text{T}$ ,  $B_0 = 14.1$  T) for different saturation lengths  $t_{\text{sat}}$  (A), duty cycles (DC) (C), pulse lengths  $t_p$  (E),  $B_1$  (G) and  $B_0$  (I). (B, D, F, H, J) Percentage variation of  $T$  at  $\Delta\omega = +3.5$  ppm. Signal dependences allow the optimization of the pulse sequence in terms of SNR. Displayed errors are the standard deviation of repeated measurements (Table S1)

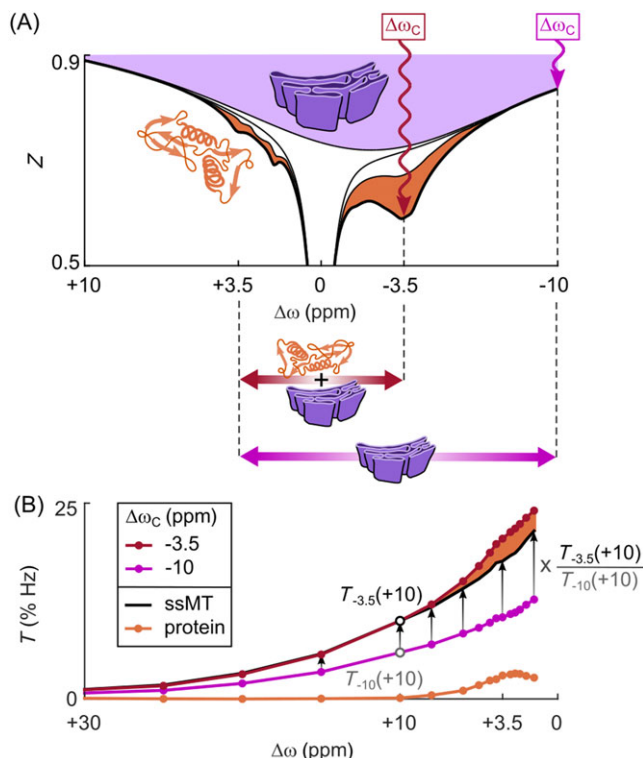


**FIGURE 4** The semi-solid magnetization transfer (ssMT) correction procedure. (A) Z-spectrum of *ex vivo* porcine brain tissue homogenate ( $B_1 = 0.75 \mu\text{T}$ ,  $B_0 = 14.1 \text{ T}$ ). The subdivision of the Z-spectrum into contributions from different cellular compounds is an estimation. By the choice of  $\Delta\omega_C$ , selectivity of the dualCEST signal to different cellular compounds can be achieved. (B) Scaling of the spectral profile of signals originating from semi-solid macromolecular structures  $T_{-10}(\Delta\omega)$  (magenta line) allows the retrieval of the isolated signal of mobile proteins  $T_{\text{protein}}$  (orange line)

### 3.3 | Characterization of the dualCEST signal

As is commonly known, signals of different cellular compounds spectrally overlap in Z-spectra *in vivo* (Figure 1B). To mimic this situation, mobile protein solutions were prepared containing: (i) BSA, as well as varying amounts of (ii) metabolites (i.e. carnosine and creatine) and (iii) lipids purified from mouse brain tissue (Figure 5). In addition to the CEST signals of BSA in the positive and negative frequency regions (Figure 5B, orange line), individual resonances of carnosine, creatine and tissue-lipids are resolved around  $\Delta\omega = +3.5$ ,  $+2.0$  and  $-3.5$  ppm, respectively (Figure 5B). In addition, a broad asymmetric ssMT of tissue-lipids is also present (Figure 5A, blue lines), completing the imitated *in vivo* Z-spectrum. The asymmetry of the ssMT can be seen in the  $\text{MTR}_{\text{asym}}$  spectra, which leads to negative values (Figure 5C). Remarkably, although Z-spectra and  $\text{MTR}_{\text{asym}}$  spectra strongly depend on the added cellular compounds, the dualCEST signal remains constant (Figure 5D). This verifies the assignment of  $T_{\text{protein}}$  to originate exclusively from mobile proteins. Furthermore,  $T_{\text{protein}}$  is compensated for changes in water signal relaxation (Figure 5E), enabling an independent investigation of bulk mobile proteins in living organisms.

To identify the physiological parameters that affect the amplitude of the dualCEST signal, mobile protein solutions were investigated under various conditions (i.e. concentration, molecular size, folding state and pH). As these model solutions did not contain any semi-solid macromolecular structures, the dualCEST signal  $T$  was evaluated without the ssMT correction procedure being applied (Equation 1). As expected,  $T$  increases as a function of mobile protein concentration (Figure 6A). The deviation from a linear increase at high concentrations,  $c > 10\%(\text{w/v})$ , most likely originates from crowding effects that influence the mobility of BSA molecules.<sup>41</sup> In addition to its obvious dependence on concentration, a considerable variation in  $T$  as a function of the molecular size, and also the protein folding state (i.e. conformation), is expected. This is the case, as the dualCEST signal arises from intramolecular spin diffusion processes that are stronger with slower tumbling of the molecules (i.e. molecular correlation time) and are weaker with increasing distances between the involved nuclei.<sup>39</sup> Indeed, a distinct increase in  $T$  as a function of the molecular weight (MW, i.e. molecular size) is observed (Figure 6B), demonstrating the potential of dualCEST to detect a decomposition of proteins into smaller fragments. For different MWs the mass concentration (i.e. protein mass per unit volume) was kept constant to exclude concentration effects. In addition, effects from different folding states of the proteins are negligible because all of the investigated proteins belong to the same class of globular proteins, which are spherical in shape. Following previous studies,<sup>42-44</sup> the equilibrium unfolding transition of BSA was examined using the detergent SDS as a denaturant and monitored by fluorescence spectroscopy (Figure 6F). Indeed, a good correlation between  $T$  and the protein folding state is observed. This illustrates the potential of dualCEST to image aberrant structural and conformational changes of proteins. Finally, the pH dependence was investigated in order to demonstrate the robustness of the dualCEST signal against changes in the chemical

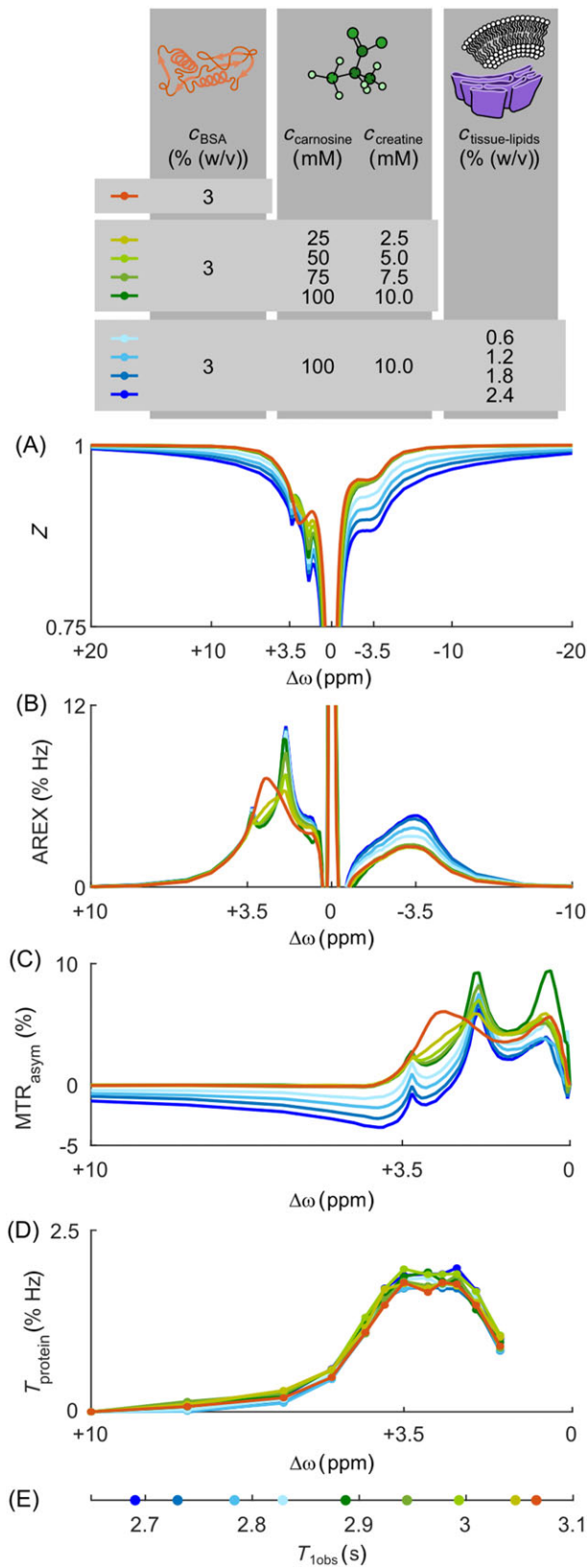


**FIGURE 5** Assignment of the dualCEST signal to mobile proteins. Z- (A), AREX (B),  $\text{MTR}_{\text{asym}}$  (C) and  $T$ -spectra (D) of BSA for varying concentrations of cellular compounds ( $\Delta\omega_{\text{C}} = -3.5$  ppm,  $B_1 = 1.5$   $\mu\text{T}$ ,  $B_0 = 14.1$  T). In contrast to conventional CEST, the signal  $T_{\text{protein}}$  can unambiguously be assigned to mobile proteins. (E) With an increasing concentration of compounds, the observed longitudinal relaxation time of water  $T_{1\text{obs}}$  is reduced



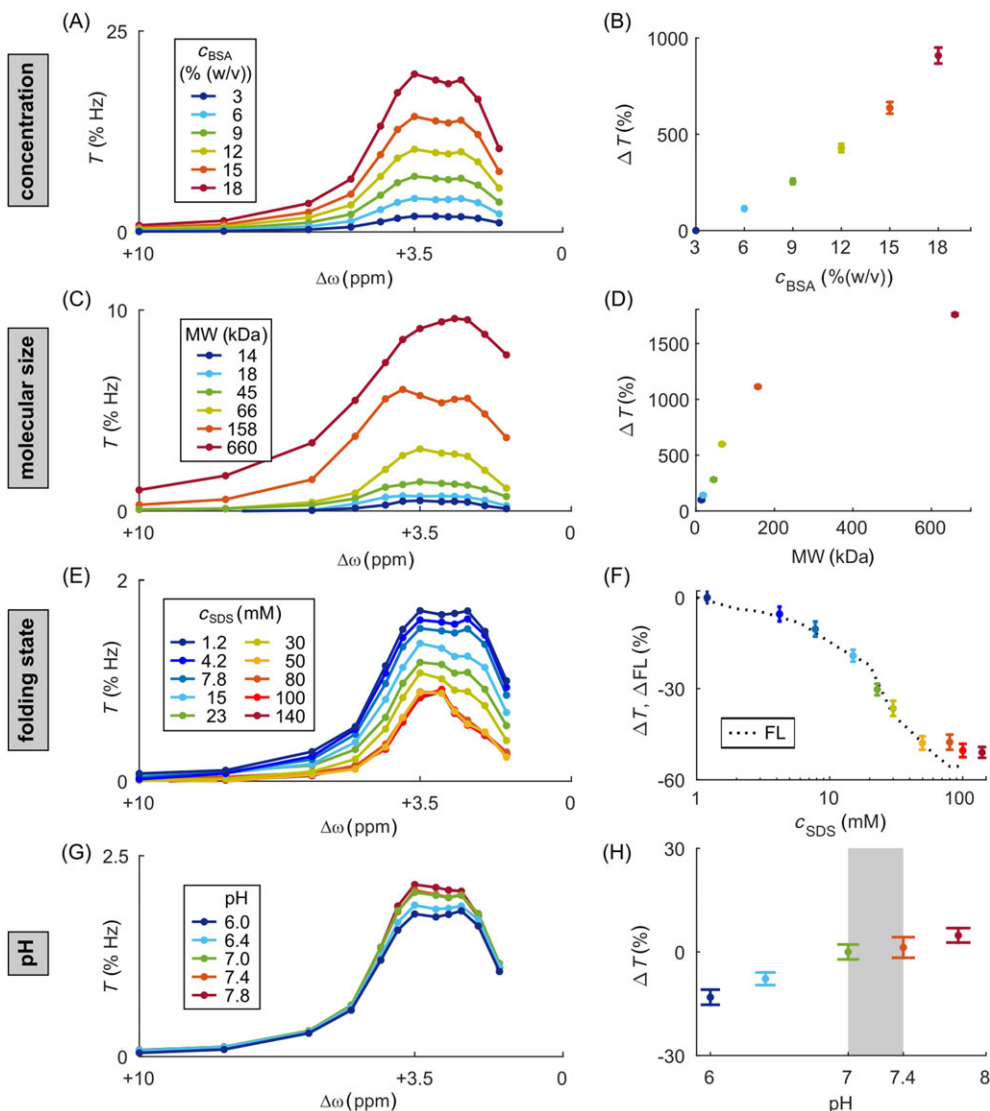


**FIGURE 6** Dependence of the dualCEST signal on physiological parameters.  $T$  spectra of BSA ( $\Delta\omega_c = -3.5$  ppm,  $B_1 = 1.5$   $\mu$ T,  $B_0 = 14.1$  T) for different concentrations (A), folding states (E) and pH (G). (C)  $T$  spectra of various globular proteins of different molecular weights (i.e. molecular sizes). (B, D, F, H) Percentage variation of  $T$  at  $\Delta\omega = +3.5$  ppm. (F) As a reference, the protein folding state was monitored by fluorescence spectroscopy (FL). Signal dependencies demonstrate that variations in  $T$  can be attributed to changes in the concentration, molecular size or folding state of mobile proteins. Displayed errors are the standard deviation of repeated measurements (Table S1)

exchange properties (i.e. exchange rate).  $T$  remains constant in the physiological range between pH 7 and 7.4 (Figure 6H, gray-shaded area), but seems to be slightly affected by a decreasing pH. Consequently, for example, pH < 7 in the extracellular tumor environment can have an influence on the dualCEST signal of secreted proteins. Deviations at acidic pH values might be a result of either the pH dependence of the chemical exchange between exchangeable protons in BSA and water,<sup>3,44</sup> or the overall BSA conformation which is also dependent on pH.<sup>41,45</sup>

Thus, in the physiological pH range, the dualCEST signal exclusively depends on the concentration, molecular size and folding state of the mobile proteins. Contributions from other cellular compounds, water relaxation properties or changes in the chemical exchange properties can be excluded. With this knowledge in hand, the dualCEST approach was utilized to investigate alterations of the mobile fraction of the proteome in a glioblastoma brain tumor.

### 3.4 | Application of dualCEST *in vivo*

For examinations in humans, the dualCEST pulse sequence was implemented on a clinical 3-T MR scanner. Transfer of the dualCEST approach to lower  $B_0$ , while maintaining its specificity to mobile proteins, is enabled by the newly introduced dimension of selectivity. As for the NMR spectrometer (Figure 3), pre-saturation parameters were optimized for the MR scanner to maximize the signal strength  $T$ , while avoiding excessive broadening of the signals.  $t_p = 20$  ms and  $B_1 = 2$   $\mu$ T were found to be optimal at  $B_0 = 3$  T. In addition, the dualCEST signal is approximately linear

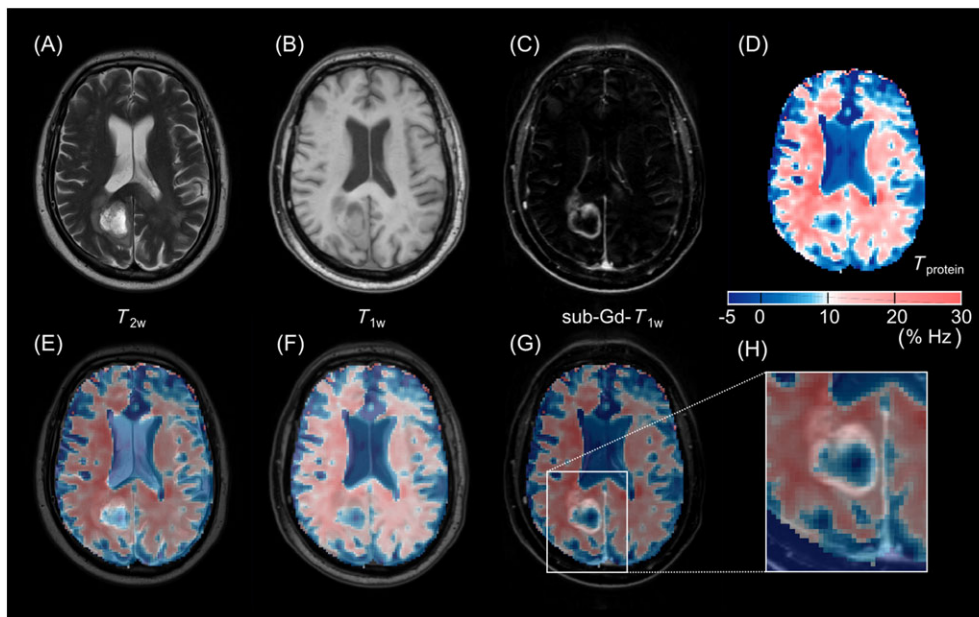


**FIGURE 7** *In vivo* dualCEST examination at  $B_0 = 3$  T. Multi-modal MR images of a patient with glioblastoma. (A–C) Conventional MR contrasts:  $T_2$ -weighted ( $T_{2w}$ ),  $T_1$ -weighted ( $T_{1w}$ ) and subtracted gadolinium contrast-enhanced  $T_1$ -weighted (sub-Gd- $T_{1w}$ ) MR images. (D) The selective dualCEST signal of mobile proteins  $T_{\text{protein}}$  showing substantial alterations of the mobile fraction of the proteome in the tumor region. (E–H) Fusion of conventional MR contrasts and the dualCEST image

as a function of  $B_1$  for the aforementioned parameters (Supporting Information Figure S3), allowing for a simple correction of  $B_1$  inhomogeneities in living tissue. However, a correction for  $B_0$  inhomogeneities is not necessary because of the comparatively broad plateau of the dualCEST resonance at 3 T around its maximum (Figure 3I, red line). To maximize the range of tolerable  $B_0$  inhomogeneities, the frequency offsets for mobile protein signals in Equation 2 were adjusted from  $\pm 3.5$  to  $\pm 5$  ppm. Moreover, the frequency offsets for ssMT signals were adjusted from  $\pm 10$  to  $\pm 30$  ppm to allow an isolated sampling of the ssMT component without contributions from mobile protein signals also at 3 T (Figure 3). Finally, the far off-resonant frequency offset in Equation 1 was adjusted from 150 to 300 ppm.

Isolated endogenous bulk mobile protein MRI of a patient with glioblastoma shows a significantly reduced signal  $T_{\text{protein}}$  in the necrotic tumor region compared with normal-appearing white matter (Figure 7H). Edges are clearly defined and show a good correlation with the inner part of the ring enhancement in the contrast media-enhanced image. The amplitude of  $T_{\text{protein}}$  in necrotic tissue is comparable with the values in cerebrospinal fluid (CSF), suggesting a considerable degeneration of the mobile fraction of the proteome in the tumor core. The specificity to mobile proteins allows the assignment of the observed signal drop to a reduced concentration, a reduced average molecular size or a denatured global folding state of bulk mobile proteins. Correct functioning of the dualCEST measurement is confirmed by signal values around zero in the CSF, where a negligible concentration of proteins can be assumed. Anatomical structures between brain matter and peripheral CSF show a good correlation with  $T_{\text{protein}}$ . In a region of interest analysis, differences in  $T_{\text{protein}}$  between gray and white matter are marginal, confirming the absence of contributions from lipids to the dualCEST signal. The equivalent signal in these two tissues is in line with data from MR spectroscopy when analyzing macromolecular resonances that are associated with bulk mobile proteins,<sup>46</sup> as well as rNOE-CEST signals evaluated by the variable delay multi-pulse (VDMP) method.<sup>47</sup> Overall, the presented *in vivo* image data verify the feasibility of dualCEST examinations in humans, enabling further investigations of the mobile fraction of the proteome in diverse pathologies.

## 4 | DISCUSSION

In this study, a novel MRI contrast is proposed, enabling the selective detection of endogenous bulk mobile proteins in living organisms. By contrast, in conventional Z-spectra *in vivo*, the CEST signals of mobile proteins spectrally overlap with signals originating from other cellular compounds (Figure 1B). Several attempts have been made in the past to overcome this obstacle and to highlight the signal component of mobile proteins. Ideas range from multi-parametric fitting,<sup>17,32,48–50</sup> to the incorporation of several types of exchange rate filters,<sup>24–26,47,51–53</sup> to the suppression of confounding signals by simultaneous pre-saturation at various frequency offsets.<sup>30,54–56</sup> Although these approaches work appropriately and allow the isolation of the prominent amide proton resonance at  $\Delta\omega = +3.5$  ppm or the rNOE-CEST signal of aliphatic protons at around  $\Delta\omega = -3.5$  ppm, the assignment of these signals exclusively to mobile proteins remains questionable. With respect to the amide proton signal, a considerable part originates from small peptides and various metabolites.<sup>57</sup> In addition, the aliphatic rNOE-CEST signal comprises contributions from other mobile macromolecules, e.g. lipids or saccharides.<sup>16,17</sup> In both cases, magnetization transfer rates to water are comparable with the rates occurring in mobile

proteins, thus preventing separation by exchange rate filtering. Here, we introduce a novel dimension of selectivity which is based on the cross magnetization transfer between two particular CEST signals – termed saturation crosstalk  $T_{\Delta\omega_c}(\Delta\omega)$ . For this purpose, the conventional CEST technique was extended to an RF irradiation scheme at two different frequency offsets. Incorporation of a saturation at an additional frequency offset was introduced for the first time in 2010.<sup>54</sup> In the following year, saturation with frequency-alternating RF irradiation (SAFARI) was proposed to avoid signal contributions from direct water saturation and ssMT.<sup>30</sup> In our study, an identical pre-saturation pulse scheme, but with different combinations of the two frequency offsets, is used to selectively detect the coupling between different CEST signals. The detection of the coupling between the CEST signal of amide and aliphatic protons provides a unique specificity to mobile proteins. In contrast, immobile proteins, such as cytoskeletal or membrane proteins, do not contribute to  $T_{\text{protein}}$ , as immobile proteins show comparatively broad signals with linewidths of several 10 ppm,<sup>57</sup> which are suppressed by the proposed ssMT correction method. As is commonly known, proton transversal relaxation times ( $T_2$ ) of immobile solid-like structures are very short (on the order of 10  $\mu\text{s}$ ) in comparison with the  $T_2$  values of mobile molecules (several 10 ms). As the linewidths of CEST signals inversely depend on  $T_2$ ,<sup>58</sup> proteins can be roughly classified by their mobility into two types – mobile and immobile.<sup>8</sup> The specificity of the dualCEST signal to mobile proteins was verified experimentally by the successive addition of different cellular compounds to a protein model solution (Figure 5). Moreover, we demonstrated that the dualCEST signal is intrinsically corrected for changes in water relaxation (i.e.  $T_{1\text{obs}}$ , Figure 5D), as well as robust against changes in the chemical exchange properties in the physiologically relevant range (i.e. pH, Figure 6H). Parameters that affect the amplitude of the dualCEST signal are the concentration, molecular size and folding state of mobile proteins (Figure 6), making dualCEST a valuable diagnostic tool to detect aberrant proteomes *in vivo*.

The largest drawback of the method is the inherently smaller SNR in comparison with conventional CEST. The reason for this is the quite large number of nine Z-values required for the calculation of the isolated mobile protein signal  $T_{\text{protein}}$  (Equation 2). However, the newly introduced dimension of selectivity opens up new possibilities to overcome this limitation. As the specificity of the dualCEST signal to mobile proteins relies on the coupling of two signals, rather than on the resolution of individual resonances, high spectral resolutions are not required. This allows the application of high  $B_1$  values to increase the signal strength without a loss of specificity (Figure 3H). In contrast, the spectral selectivity clearly deteriorates when acquiring conventional Z-spectra using high  $B_1$  because of extensive peak broadening. Other possibilities to further amplify the dual CEST signal were found to be the reduction in  $t_p$  (Figure 3F) and  $B_0$  (Figure 3J). The signal amplification at shorter  $t_p$  can be attributed to the expansion of the spectral bandwidth of the pre-saturation pulses and the concomitant incorporation of more protons from neighboring chemical shifts into the measurement procedure. This is because, in proteins, the chemical shift of identical proton types (e.g. amides) is dispersed, depending on their location inside the protein and the respective chemical environment.<sup>59</sup> In a similar manner, the number of saturated protons, and thus the signal strength, is also increased by reducing the spectral resolution (i.e. reducing  $B_0$ ). Consequently, the dualCEST signal profits from lower magnetic field strengths, paving the way for dualCEST examinations on clinical MR scanners. In this study, *in vivo* measurements were performed at a magnetic field strength of 3 T and optimized to maximize the signal amplitude, while avoiding an excessive broadening of the signals. Linewidths broader than the distance between the two frequency offsets  $\Delta\omega$  and  $\Delta\omega_c$  might cause a direct saturation of CEST signals at one frequency offset induced by pulses applied at the other. This might influence the signal preparation, leading to disturbed dualCEST signals. However, the utilized distance of 10 ppm at 3 T between  $\Delta\omega$  and  $\Delta\omega_c$  should be sufficient to avoid such influences, assuming that the linewidths of the individual CEST pools do not exceed 20 ppm. These features should have allowed the acquisition of dualCEST images with adequate SNR. However, there were technical limitations of the MR scanner used in this work which prevented a pre-saturation with an ideal DC of 50% (please note: these limitations were caused by the restricted amplifier performance and not the specific absorption rate, SAR). Instead, only a DC of approximately half the desired value could be realized, which is why several repetitions were required to acquire a reliable dualCEST image *in vivo*.

For repeated measurements, the dualCEST approach profits from a fast and direct acquisition. By 'direct', we mean that  $T_{\Delta\omega_c}(\Delta\omega)$  can be calculated from unprocessed data without the application of any fitting procedure to approximate the direct water saturation or ssMT. This allows a fast determination of the dualCEST signal without the need for the sampling of an entire spectrum, leading to a considerable saving in acquisition time. Exclusion of the fitting procedure was enabled by an analytical description based on the AREX<sup>36</sup> evaluation (Figure S1). In this theory,  $T_{\Delta\omega_c}(\Delta\omega)$  is a correction term – considering the exchange of magnetization between two different CEST pools – which is added to the longitudinal relaxation rate in the rotating frame  $R_{1\rho}$  of a multi-pool system.<sup>58,60,61</sup> The validity of the analytical model requires a saturation length in compliance with the criterion for steady state (Figure 3B). In addition, the tilt angle  $\theta$  of the effective field and the z-axis must be small in

compliance with:  $\cos^2\theta = \frac{\Delta\omega^2}{\Delta\omega^2 + (\gamma B_1)^2} \approx 1$ .<sup>21,36,58</sup> This limits the evaluation of signals at small  $\Delta\omega$  when applying comparatively high  $B_1$ . Violation of this assumption leads to strong signal distortions, as observed at  $\Delta\omega < 2.75$  ppm when acquiring signals at  $B_0 = 3$  T and  $B_1 = 2$   $\mu\text{T}$  (Figure 3I, red line). The saving in acquisition time allowed the repetition of the acquisitions to accumulate sufficient SNR for dualCEST examinations of a brain tumor patient without impractical lengthening of the measurement time.

The dualCEST approach allows the identification of pathological modifications of the mobile fraction of the proteome *in vivo*. Significant changes in the isolated mobile protein signal  $T_{\text{protein}}$  were detected in the necrotic region of a human brain tumor (Figure 7). Necrotic tissue is known to consist of decomposing or dead cells, verifying the ability of the dualCEST signal to detect aberrant proteomes in living organisms. In the future, whole cohorts of patients will need to be examined to reliably determine the actual contribution of mobile proteins to CEST signal changes in different pathologies, and to further investigate the diagnostic value of the presented method. As  $T_{\text{protein}}$  is a quantitative value, a comparison between different subjects is possible. Applications range from staging and follow-up studies of cancer treatment to the diagnosis of neurodegenerative diseases associated with the accumulation of pathogenic protein plaques, e.g. Alzheimer's disease. In addition, the dualCEST

approach should be particularly suitable for the selective detection of binding mechanisms of mobile proteins, as its specificity relies on the coupling of different CEST signals. In this context, selective imaging of small exogenous CEST agents binding to mobile proteins is plausible because of the immobilization of the small molecules and the resulting intermolecular magnetization transfer pathway.<sup>62</sup>

## 5 | CONCLUSIONS

A novel MRI technique – termed dualCEST – is proposed, allowing the selective detection of endogenous bulk mobile proteins in humans. In this study, for the first time, the coupling of different CEST signals mediated by intramolecular spin diffusion is exploited to introduce an exceptional specificity into the CEST experiment. The specificity of the dualCEST signal to bulk mobile proteins was verified experimentally by the investigation of different cellular compounds under different physiological conditions. A fast and direct acquisition of the dualCEST signal was enabled by an analytical description of the dualCEST signal. With regard to applications in humans, the dualCEST signal was maximized by a comprehensive study of diverse technical parameters. Remarkably, it was found that the dualCEST signal profits from lower magnetic field strengths, allowing a straightforward implementation of dualCEST examinations on clinical MR scanners. The applicability of the dualCEST technique for examinations in humans was verified in a proof-of-principle study of a brain tumor patient at 3 T.

## ACKNOWLEDGEMENTS

We cordially thank Enza di Gregorio and Francesca Garello from the Department of Molecular Biotechnology and Health Sciences at the University of Turin in Italy for the extraction of lipids and liposome preparation. The authors declare no conflicts of interest.

## ORCID

Steffen Goerke  <http://orcid.org/0000-0002-0684-2423>

Moritz Zaiss  <http://orcid.org/0000-0001-9780-3616>

Dario L. Longo  <http://orcid.org/0000-0002-6906-9925>

## REFERENCES

1. Wolff SD, Balaban RS. NMR imaging of labile proton exchange. *J Magn Reson.* 1990;86:164-169.
2. Ward KM, Balaban RS. Determination of pH using water protons and chemical exchange dependent saturation transfer (CEST). *Magn Reson Med.* 2000;44:799-802.
3. Zhou J, van Zijl PCM. Chemical exchange saturation transfer imaging and spectroscopy. *Prog Nucl Magn Reson Spectrosc.* 2006;48:109-136.
4. McMahon MT, Gilad AA, Bulte JWM, van Zijl PCM. *Chemical Exchange Saturation Transfer Imaging: Advances and Applications.* 1st ed. Singapore: Pan Stanford Publishing Pte Ltd; 2017.
5. van Zijl PCM, Lam WW, Xu J, Knutsson L, Stanisz GJ. Magnetization transfer contrast and chemical exchange saturation transfer MRI. Features and analysis of the field-dependent saturation spectrum. *NeuroImage.* 2017;168:222-241.
6. Zhou J, Payen J-F, Wilson DA, Traystman RJ, van Zijl PCM. Using the amide proton signals of intracellular proteins and peptides to detect pH effects in MRI. *Nat Med.* 2003;9:1085-1090.
7. Zhou J, Lal B, Wilson DA, Laterra J, van Zijl PCM. Amide proton transfer (APT) contrast for imaging of brain tumors. *Magn Reson Med.* 2003;50:1120-1126.
8. Yan K, Fu Z, Yang C, et al. Assessing amide proton transfer (APT) MRI contrast origins in 9 L gliosarcoma in the rat brain using proteomic analysis. *Mol Imaging Biol.* 2015;17:479-487.
9. Zaiss M, Windschuh J, Goerke S, et al. Downfield-NOE-suppressed amide-CEST-MRI at 7 Tesla provides a unique contrast in human glioblastoma. *Magn Reson Med.* 2017;77:196-208.
10. Cai K, Haris M, Singh A, et al. Magnetic resonance imaging of glutamate. *Nat Med.* 2012;18:302-307.
11. Haris M, Nanga RPR, Singh A, et al. Exchange rates of creatine kinase metabolites: feasibility of imaging creatine by chemical exchange saturation transfer MRI. *NMR Biomed.* 2012;25:1305-1309.
12. Rerich E, Zaiss M, Korzowski A, Ladd ME, Bachert P. Relaxation-compensated CEST-MRI at 7 T for mapping of creatine content and pH – preliminary application in human muscle tissue *in vivo.* *NMR Biomed.* 2015;28:1402-1412.
13. Chan KWY, McMahon MT, Kato Y, et al. Natural D-glucose as a biodegradable MRI contrast agent for detecting cancer. *Magn Reson Med.* 2012;68:1764-1773.
14. Walker-Samuel S, Ramasawmy R, Torrealdea F, et al. In vivo imaging of glucose uptake and metabolism in tumors. *Nat Med.* 2013;19:1067-1072.
15. Schuenke P, Paech D, Koehler C, et al. Fast and quantitative T1 $\rho$ -weighted dynamic glucose enhanced MRI. *Sci Rep.* 2017;7:42093.
16. van Zijl PCM, Zhou J, Mori N, Payen J-F, Wilson D, Mori S. Mechanism of magnetization transfer during on-resonance water saturation. a new approach to detect mobile proteins, peptides, and lipids. *Magn Reson Med.* 2003;49:440-449.
17. Jones CK, Huang A, Xu J, et al. Nuclear Overhauser enhancement (NOE) imaging in the human brain at 7 T. *NeuroImage.* 2013;77:114-124.
18. Henkelman RM, Stanisz GJ, Graham SJ. Magnetization transfer in MRI: a review. *NMR Biomed.* 2001;14:57-64.
19. Henkelman RM, Huang X, Xiang Q-S, Stanisz GJ, Swanson SD, Bronskill MJ. Quantitative interpretation of magnetization transfer. *Magn Reson Med.* 1993;29:759-766.
20. Zaiss M, Zu Z, Xu J, et al. A combined analytical solution for chemical exchange saturation transfer and semi-solid magnetization transfer. *NMR Biomed.* 2015;28:217-230.

21. Goerke S, Zaiss M, Bachert P. Characterization of creatine guanidinium proton exchange by water-exchange (WEX) spectroscopy for absolute-pH CEST imaging in vitro. *NMR Biomed*. 2014;27:507-518.
22. Liepinsh E, Otting G. Proton exchange rates from amino acid side chains—implications for image contrast. *Magn Reson Med*. 1996;35:30-42.
23. Bai Y, Milne JS, Mayne L, Englander SW. Primary structure effects on peptide group hydrogen exchange. *Proteins Struct Funct Genet*. 1993;17:75-86.
24. Friedman JI, McMahon MT, Stivers JT, van Zijl PCM. Indirect detection of labile solute proton spectra via the water signal using frequency-labeled exchange (FLEX) transfer. *J Am Chem Soc*. 2010;132:1813-1815.
25. Zu Z, Janve VA, Xu J, Does MD, Gore JC, Gochberg DF. A new method for detecting exchanging amide protons using chemical exchange rotation transfer. *Magn Reson Med*. 2013;69:637-647.
26. Xu J, Yadav NN, Bar-Shir A, et al. Variable delay multi-pulse train for fast chemical exchange saturation transfer and relayed-nuclear Overhauser enhancement MRI. *Magn Reson Med*. 2014;71:1798-1812.
27. Jones CK, Schlosser MJ, van Zijl PCM, Pomper MG, Golay X, Zhou J. Amide proton transfer imaging of human brain tumors at 3T. *Magn Reson Med*. 2006;56:585-592.
28. Wen Z, Hu S, Huang F, et al. MR imaging of high-grade brain tumors using endogenous protein and peptide-based contrast. *Neuroimage*. 2010;51:616-622.
29. Jia G, Abaza R, Williams JD, et al. Amide proton transfer MR imaging of prostate cancer: a preliminary study. *J Magn Reson Imaging*. 2011;33:647-654.
30. Scheidegger R, Vinogradov E, Alsop DC. Amide proton transfer imaging with improved robustness to magnetic field inhomogeneity and magnetization transfer asymmetry using saturation with frequency alternating RF irradiation. *Magn Reson Med*. 2011;66:1275-1285.
31. Zhou J, Yan K, Zhu H. A simple model for understanding the origin of the amide proton transfer MRI signal in tissue. *Appl Magn Reson*. 2012;42:393-402.
32. Zaiss M, Windschuh J, Paech D, et al. Relaxation-compensated CEST-MRI of the human brain at 7 T: unbiased insight into NOE and amide signal changes in human glioblastoma. *Neuroimage*. 2015;112:180-188.
33. Heo H-Y, Jones CK, Hua J, et al. Whole-brain amide proton transfer (APT) and nuclear Overhauser enhancement (NOE) imaging in glioma patients using low-power steady-state pulsed chemical exchange saturation transfer (CEST) imaging at 7T. *J Magn Reson Imaging*. 2016;44:41-50.
34. Zhou J, Tryggstad E, Wen Z, et al. Differentiation between glioma and radiation necrosis using molecular magnetic resonance imaging of endogenous proteins and peptides. *Nat Med*. 2011;17:130-134.
35. Mehrabian H, Desmond KL, Soliman H, Sahgal A, Stanisz GJ. Differentiation between radiation necrosis and tumor progression using chemical exchange saturation transfer. *Clin Cancer Res*. 2017;23:3667-3675.
36. Zaiss M, Xu J, Goerke S, et al. Inverse Z-spectrum analysis for spillover-, MT-, and T1-corrected steady-state pulsed CEST-MRI – application to pH-weighted MRI of acute stroke. *NMR Biomed*. 2014;27:240-252.
37. Windschuh J, Zaiss M, Meissner J-E, et al. Correction of B1-inhomogeneities for relaxation-compensated CEST imaging at 7 T. *NMR Biomed*. 2015;28:529-537.
38. Schuenke P, Windschuh J, Roeloffs V, Ladd ME, Bachert P, Zaiss M. Simultaneous mapping of water shift and B1 (WASABI)—application to field-inhomogeneity correction of CEST MRI data. *Magn Reson Med*. 2017;77:571-580.
39. Neuhaus D, Williamson MP. *The Nuclear Overhauser Effect in Structural and Conformational Analysis*. New York: Wiley; 1989.
40. van Zijl PCM, Yadav NN. Chemical exchange saturation transfer (CEST): what is in a name and what isn't? *Magn Reson Med*. 2011;65:927-948.
41. Barbosa LRS, Ortore MG, Spinozzi F, Mariani P, Bernstorff S, Itri R. The importance of protein-protein interactions on the pH-induced conformational changes of bovine serum albumin: a small-angle X-ray scattering study. *Biophys J*. 2010;98:147-157.
42. Zaiss M, Kunz P, Goerke S, Radbruch A, Bachert P. MR imaging of protein folding in vitro employing nuclear-Overhauser-mediated saturation transfer. *NMR Biomed*. 2013;26:1815-1822.
43. Longo DL, Gregorio ED, Abategiovanni R, et al. Chemical exchange saturation transfer (CEST): an efficient tool for detecting molecular information on proteins' behaviour. *Analyst*. 2014;139:2687-2690.
44. Goerke S, Zaiss M, Kunz P, et al. Signature of protein unfolding in chemical exchange saturation transfer imaging. *NMR Biomed*. 2015;28:906-913.
45. Lin VJC, Koenig JL. Raman studies of bovine serum albumin. *Biopolymers*. 1976;15:203-218.
46. Snoussi K, Gillen JS, Horska A, et al. Comparison of brain gray and white matter macromolecule resonances at 3 and 7 Tesla. *Magn Reson Med*. 2015;74:607-613.
47. Xu X, Yadav NN, Zeng H, et al. Magnetization transfer contrast-suppressed imaging of amide proton transfer and relayed nuclear Overhauser enhancement chemical exchange saturation transfer effects in the human brain at 7T. *Magn Reson Med*. 2016;75:88-96.
48. Desmond KL, Moosvi F, Stanisz GJ. Mapping of amide, amine, and aliphatic peaks in the CEST spectra of murine xenografts at 7 T. *Magn Reson Med*. 2013;71:1841-1853.
49. Heo H-Y, Zhang Y, Lee D-H, Hong X, Zhou J. Quantitative assessment of amide proton transfer (APT) and nuclear Overhauser enhancement (NOE) imaging with extrapolated semi-solid magnetization transfer reference (EMR) signals: application to a rat glioma model at 4.7 tesla. *Magn Reson Med*. 2016;75:137-149.
50. Zhou IY, Wang E, Cheung JS, Zhang X, Fulci G, Sun PZ. Quantitative chemical exchange saturation transfer (CEST) MRI of glioma using Image Downsampling Expedited Adaptive Least-squares (IDEAL) fitting. *Sci Rep*. 2017;7:84.
51. Zu Z, Janve VA, Li K, Does MD, Gore JC, Gochberg DF. Multi-angle ratiometric approach to measure chemical exchange in amide proton transfer imaging. *Magn Reson Med*. 2012;68:711-719.
52. Xu J, Chan KWY, Xu X, Yadav N, Liu G, van Zijl PCM. On-resonance variable delay multipulse scheme for imaging of fast-exchanging protons and semisolid macromolecules. *Magn Reson Med*. 2017;77:730-739.
53. Lin C-Y, Yadav NN, Friedman JI, Ratnakar J, Sherry AD, van Zijl PCM. Using frequency-labeled exchange transfer to separate out conventional magnetization transfer effects from exchange transfer effects when detecting ParaCEST agents. *Magn Reson Med*. 2012;67:906-911.
54. Närviäinen J, Hubbard PL, Kauppinen RA, Morris GA. Z-spectroscopy with alternating-phase irradiation. *J Magn Reson*. 2010;207:242-250.
55. Lee J-S, Regatte RR, Jerschow A. Isolating chemical exchange saturation transfer contrast from magnetization transfer asymmetry under two-frequency rf irradiation. *J Magn Reson*. 2012;215:56-63.

56. Friedman JI, Xia D, Regatte RR, Jerschow A. Transfer rate edited experiment for the selective detection of chemical exchange via saturation transfer (TRE-CEST). *J Magn Reson.* 2015;256:43-51.
57. Goerke S, Milde KS, Bukowiecki R, et al. Aggregation-induced changes in the chemical exchange saturation transfer (CEST) signals of proteins. *NMR Biomed.* 2017;30:e3665.
58. Zaiss M, Bachert P. Chemical exchange saturation transfer (CEST) and MR Z-spectroscopy in vivo: a review of theoretical approaches and methods. *Phys Med Biol.* 2013;58:R221-R269.
59. Wüthrich K. *NMR of Proteins and Nucleic Acids.* New York: John Wiley & Sons; 1986.
60. Zaiss M, Bachert P. Exchange-dependent relaxation in the rotating frame for slow and intermediate exchange - modeling off-resonant spin-lock and chemical exchange saturation transfer. *NMR Biomed.* 2013;26:507-518.
61. Trott O, Palmer AG III. Theoretical study of R1 $\rho$  rotating-frame and R2 free-precession relaxation in the presence of n-site chemical exchange. *J Magn Reson.* 2004;170:104-112.
62. Yadav NN, Yang X, Li Y, Li W, Liu G, Zijl PCM. Detection of dynamic substrate binding using MRI. *Sci Rep.* 2017;7:10138.

## SUPPORTING INFORMATION

Additional Supporting Information may be found online in the supporting information tab for this article.

**How to cite this article:** Goerke S, Breitling J, Zaiss M, et al. Dual-frequency irradiation CEST-MRI of endogenous bulk mobile proteins. *NMR in Biomedicine.* 2018;31:e3920. <https://doi.org/10.1002/nbm.3920>